A High Precison Phase Extraction Algorithm from a Single Shot Interferogram

Lifa Hu[1,2,*], Wen Shen[1,2], Wenchao Ma[1,2], Dongting Hu[1,2] and Xinyu Liu[1,2]

[1]Jiangnan University, School of Science, Department of Photoelectric Information Science and Engineering, Wuxi, China, 214122

[2]Jiangnan University, Jiangsu Provincial Research Center of Light Industrial Optoelectronic Engineering and Technology, Wuxi, China, 214122

Abstract. Phase shifting interferometry is an optical metrology with a high precision, but it usually requires the expensive high precision phase shifter. Therefore, low cost methods of extracting phase from a single shot interferogram were very valuable, but available algorithms are usually effective only in a limited conditions. To solve these problems, a novel method is presented in this work. Based on this method, the interference fringe is retrieved to a wrapped phase and divided into different regions and the index of the pixel is calculated. The pixels in the same region have the same parity and the PSF's gravity center of part wavefront so as to solve the sign ambiguity. The theoretical simulation results indicate that the PV of wavefront error is 0.00054λ and the rms is 0.000125λ,which is much better than the results from the Fast Fourier Transformation method. The experimentally measured interferogram is also used to validate the method. It has the advantages of simplicity, high precision and effective for both open and closed interferometer fringes.

Keywords: Interferometer, Wavefront measurement.

1. INTRODUCTION

The optical interferometry is widely used for precision measurements, surface diagnostics, astrophysics, seismology, quantum information, etc [1]. According to their data processing algorithms, they can be divided into two types. One is to measure the variation of the interference fringe or the optical path difference at a specified point on the interference field to obtain the sample parameters, such as size, displacement, material micro-deformation and refractive index. The other is to obtain surface shape, sample geometry or fluid density distribution by measuring the interference fringes generated by the measured wavefront and the reference standard wavefront. Surface shape measurement is the classic applications of the optical interferometry.

Generally, there are mainly two algorithms used to extract phase from interference fringes. The first is the phase shifting method as used in many optical interferometers [1-4]. It requires a high-precision phase shifter that is used to produce several interferograms with fixed phase step in sequence, or uses complex optical layout to generate interferograms with fixed phase differences in different sub-areas of CCD. Therefore, high phase demodulation accuracy can be obtained. But it can only be used in static or quasi-static situations. In order to overcome the problem, real-time phase shifting interference technology has been investigated [5, 6], but the presented optical system is complex and costly, which limits its application.

The second is to extract the phase from a single shot interferometer fringe, for example, wavelet analysis [6-9], Hilbert transform [10-15], fast Fourier transform [16-19], regularized phase tracing method [20-22] and the energy minimization method [23-25] and so on. Compared with the phase shifting method, it does not require precise phase shifting devices and multiple interference fringes, and the phase distribution can be recovered by single shot interference fringe, and it is valuable for the study of transient or dynamic problems.

The above methods for single shot interferogram is effective to solve the global ambiguity. However, to solve the sign ambiguity, these methods need prior knowledge. For example, the interferometric image will show dry areas for breaking up tear film where phase is the absolutely zero [24]. The prior knowledge is key for the measurement. And the monotonous characteristics because of a carrier frequency is also very important as the valuable prior knowledge to solve the sign ambiguity [16].

In addition, among these methods, the most popular is the fast Fourier transform method (FFT), which realizes the demodulation of interference fringes by adding large tilt to the interference fringe to be

*Address correspondence to this author at the Jiangnan University, School of Science, Department of Photoelectric Information Science and Engineering, Wuxi, China, 214122; E-mail: hulifa@jiangnan.edu.cn

E-ISSN: 2409-9848/23 © 2023 Zeal Press

measured. In order to improve the phase extraction accuracy, reasonable parameters of the carrier frequency and window function are very important, but also resulting in complicated calculation. In addition, it is easy to generate unreasonable phase truncation and spectral aliasing for closed fringes, which limits its application.

In the paper, a simple and effective data processing method is presented to solve the global sign ambiguity. The basic idea is to calculate the wrapped phase according to the relationship between fringe intensity and phase, then extract the unwrapped phase according to the odd or even regions. Theoretical simulation with our method and experimental cases are presented in detail. It is simple and effective to calculate the wavefront with high precision, and does not require a carrier frequency function, a Fourier transform or a Hilbert transform.

In this research, we propose a parity method to extract the phase from a single fringe pattern theoretically and experimentally. In section 2, the principle and specific steps of the method are presented. In section 3, the phase extraction accuracy of the method are theoretically investigated and compared with those of FFT method. Finally, section 4 summarizes this research.

2. THE THEORETICAL FOUNDATION

In the classic Michelson interferometer, the aberration of the optical surface to be measured, or its certain inclination angle relative to reference mirror, will cause the optical path difference between the reflected light beams on the interferometer's two surfaces. It will make the interference fringes bent or change their density. The intensity of light or interference fringe acquired by the camera can be described as

$$I = I_1 + I_2 + 2\sqrt{I_1 I_2}\cos(\Delta\phi) \tag{1}$$

Where I_1 and I_2 are the light intensities of the two beams of the interferometer, respectively; $\Delta\phi$ is the phase difference between the surface to be measured and the reference plane. It should be noted that considering the reflection mode of the interferometer, the phase in the cosine function is twice of the actual wavefront. In general, when the light intensity of the two beams is the same as I_0, the light intensity can be computed from equation (1) as:

$$I = 2I_0\left[1 + \cos(\Delta\phi)\right] \tag{2}$$

Generally, the light field distribution in experiments is filtered and normalized to improve the sign noise ratio (SNR) to extract the phase [26]. According to equation (2), we define a normalized intensity I_{norm} at point (x,y) as:

$$I_{norm}(x, y) = \frac{I}{4I_0} = 0.5 + 0.5\cos\left[\Delta\phi(x, y)\right] \tag{3}$$

Where, the value of normalized intensity I_{norm} obtained by equation (3) is ranged from 0 to 1. For a 8-bit CCD, we could define a monotonous relationship between the normalized light intensity I_{norm} and the gray level I_{linear} as follows :

$$I_{linear}(x, y) = 255 \cdot I_{norm}(x, y) \tag{4}$$

Where $0 \le I_{linear} \le 255$, and the normalized light intensity is equal to cos(ΔΦ). Therefore, the phase as a function of the light intensity I_{linear} according to equations (3) and (4) is computed as:

$$\Delta\phi_\pi(x, y) = a\cos\left[I_{norm}(x, y)\right] = a\cos\left[\frac{2}{255}I_{linear}(x, y) - 1\right] \tag{5}$$

It should be noted that the phase obtained from equation (5) is ranged from 0 to π. For the 8-bit camera with a maximum light intensity of 255, the gray level as a function of the phase corresponding to the light intensity I_{linear} is shown in Figure **1**. The abscissa is the gray value of the fringe with 8-bit. The maximum gray value is 255 and the minimum is 0, and the phase in Y-axis is ranged from 0 to π. Using the data of Figure **1**, a look-up table (LUT) including phase and light intensity can be used to compute the wrapped phase from a normalized single fringe pattern.

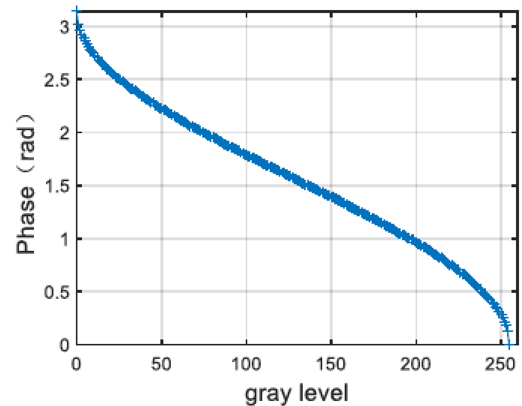

Figure 1: Relationship between phase and gray level.

A classic Michelson interferometer is shown in Figure **2**(**a**). And a simple fringe pattern as an example

is generated based on the Zernike polynomial on the unit circle as shown in Figure **2**(**b**), and the coefficients of simulated Zernike tip and tilt terms is -1.4λ, and λ=635nm. Correspondingly, its PV and RMS of wavefront are 6.23λand 1.56λ, respectively. The simulated interference fringe pattern with a grid number of 256x256 is shown in Figure **2**. The black area corresponds to the zero gray level and the white one corresponds to the gray level of 255. Therefore, from the interferogram, we can calculate its phase $\Delta\Phi_\pi$ according to equation (5).

In order to obtain the wrapped phase from 0 to 2π from the phase $\Delta\Phi_\pi$, we could use the following data processing steps: First, define a matrix $n_{i,j}$ that is used to record the characteristic values of every pixels of the fringe pattern, i and j are the row and column number of the fringe pattern, respectively; Second, find the locally darkest and brightest pixels from the fringe pattern, and then set $n_{i,j}$ to -1 and 1, respectively, and the rest pixel's values are set to zero. The obtained $n_{i,j}$ is shown in Figure **3**. Therefore, the fringe pattern could be divided into different areas according to the lines in Figure **3**.

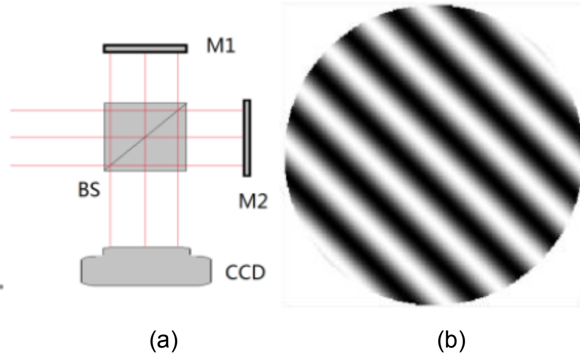

(a) (b)

Figure 2: (**a**) Schematic diagram of optical layout, M1: reference mirror; M2: mirror to be measured; BS: beam splitter; (**b**) simulated interference fringe pattern.

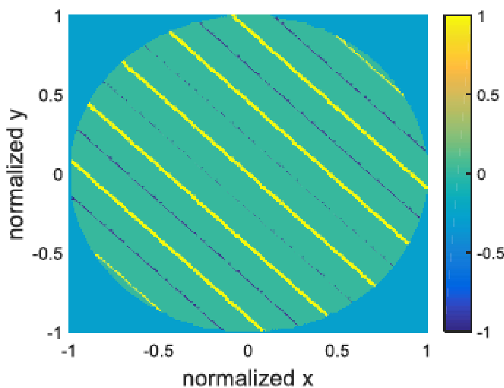

Figure 3: The obtained $n_{i,j}$, the brightest(yellow) and darkest (blue) part of the fringe pattern are for 1 and -1, respectively.

Additionally, set a value $m_{i,j}$ to every pixel in the unit circle from left to right and bottom to top:

$$m_{i,j} = p_i + k_{i,j} \tag{6}$$

Where p_i is the value of the first pixel of every row in the unit circle. And it is zero for the first pixel of the first row in the unit circle, and when it passes a peak or valley for the first pixel of the i-th row in the unit circle from bottom to top of Figure **3**, pi increases by one. $k_{i,j}$ is zero for the first pixel of every rows in the unit circle shown in Figure **3**, and then $k_{i,j}$ increases by one when a peak or valley is passed from left to right on the basis of p_i for the next pixels of every rows in the unit circle. Therefore, according to equation (6), it will be obvious that $m_{i,j}$ for the pixels in the area between the adjacent peak and valley lines as shown in Figure **3** will be the same parity.

With the $m_{i,j}$ value of each pixel according to equation (6), phase $\Delta\Phi_\pi$ could be transformed to wrapped phase $\Delta\Phi_{2\pi}$ as follows:

$$\Delta\phi_{2\pi}\left(x, y\right) = \left(-1\right)^{n_{i,j}} \Delta\phi_{\pi}\left(x, y\right) + \pi \tag{7}$$

Where $\Delta\Phi_{2\pi}$ is ranged from 0 to 2π. Since any two adjacent points usually have a continuous phase and their phase difference is smaller. A phase shift of 2π is added when their phase difference is larger than π. Then, we obtain the unwrapped phase according to the phase difference between the two adjacent pixels, which solve the ambiguity. After that, the unwrapped phase usually may have errors especially for some points with large phase difference. Therefore, we have to fit the result with Zernike polynomial to improve the accuracy of phase recovery. The used Zernike polynomial is defined as follow [27]:

$$Z = \begin{cases} Z_{even,i} = \sqrt{n+1}R_n^m(r)\sqrt{2}\cos(m\theta), m \neq 0 \\ Z_{odd,i} = \sqrt{n+1}R_n^m(r)\sqrt{2}\sin(m\theta), m \neq 0 \\ Z_{even,i} = \sqrt{n+1}R_n^0(r), m = 0 \end{cases} \tag{8}$$

$$R_n^m(r) = \sum_{s=0}^{(n-m)/2} \frac{(-1)^s(n-s)!}{s![(n+m)/2-s]![(n-m)/2-s]!} r^{n-2s}, m \neq 0$$

Where both the radial order n and the angular order m are integers, and $m \leqq n$ and (n-|m|) is even. Arbitrary wavefront can be as follows:

$$\phi = \sum_{i=1}^{M} C_i \cdot Z_i \tag{9}$$

Where C_i is the coefficient of the i-th Zernike mode Z_i; the total number of Zernike modes fitted is M; the total number of grid points is K; And the first term of Zernike polynomials, piston, is not considered. The above formula can be written as follows:

$$[\phi_1 \ \ \phi_2 \ \ \cdots \ \ \phi_K] = [C_1 \ \ C_2 \ \ \cdots \ \ C_M] \cdot \begin{bmatrix} Z_{1,1} & Z_{1,2} & \cdots & Z_{1,K} \\ Z_{2,1} & Z_{2,2} & \cdots & Z_{2,K} \\ \vdots & \vdots & \ddots & \vdots \\ Z_{M,1} & Z_{M,2} & \cdots & Z_{M,K} \end{bmatrix} \quad (10)$$

Therefore, the coefficient vector C could be calculated as follow:

$$C = \phi \cdot pinv(Z) \quad (11)$$

Where C and Z are the coefficient vector and the Zernike mode matrix in equation (10), respectively. Therefore, the fitted wavefront is obtained from the unwrapped phase as follow:

$$\Delta\phi_{fitted} = \left[\Delta\phi_{unwrapped} \cdot pinv(Z)\right] \cdot Z \quad (12)$$

Considering the reflective structure of the interferometer, the wavefront to be measured should be half of the result from the above formula:

$$\Delta\phi_{meas} = 0.5 \cdot \left[\Delta\phi_{wrapped} \cdot pinv(Z)\right] \cdot Z \quad (13)$$

In fact, when calculating the simulated interference fringes, taking the Michelson interferometer structure, the amplitude of the reflected wavefront is twice that of the shape to be measured.

To solve the sign ambiguity, we could use a part of the reconstructed wavefront to estimate its PSF(point spread function, PSF). Then, its centers along x and y axis are calculated and compared with the measured one, which is used as the prior knowledge to solve the sign ambiguity. In the simulation, we could use the up left circular area with its center in the center of the up left quarter of the whole area and its diameter is half of the whole one. Different global tilt and tip in the selected circular area will make the gravity center of estimated PSF have different positions, which could be used as the prior knowledge to solve the global sign ambiguity. Experimentally, we could use a hole and a lens in Figure **2**(**a**) and remove M1 as shown in Figure **4**. If there are obvious differences between the gravity center positions of the measured one and the estimated one, the local tilt and tip of the selected part in estimated wavefront is in a wrong direction, which will be used as a prior knowledge to solve the global sign ambiguity. In fact, during the large aperture aspheric surface processing, their surface is continuously changed and it is not necessary to judge the global sign as shown in Figure **4** every time.

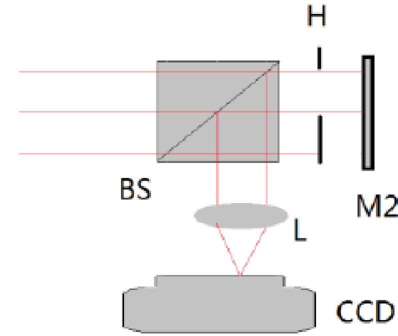

Figure 4: PSF measurement of selected part surface of M2, M2: mirror to be measured; BS: beam splitter; H: hole; L: lens.

3. SIMULATION AND DISCUSSION

In Section 2, we use the tilt term to introduce the data processing procedure in detail. The main procedure is also described in section 2. We find the peak or vale trace of the fringe pattern, and then set the index $p_{i,j}$ to every pixel according to equation (6). In addition, we further improve the accuracy of phase recovery by Zernike polynomials fitting. Finally, we verify the presented method by a theoretical simulation. To evaluate the precision of restoring the phase from a single fringe, we calculate the residual wavefront as:

$$\Delta\phi_{err} = \Delta\phi_{origin} - \Delta\phi_{meas} \quad (14)$$

Where $\Delta\Phi_{origin}$ and $\Delta\Phi_{meas}$ are the original wavefront and the measured one, respectively.

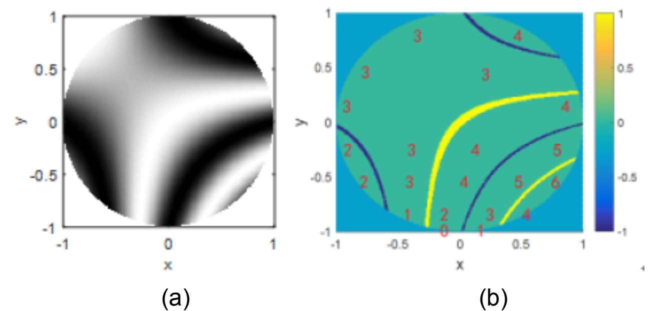

Figure 5: Parity of $p_{i,j}$ in different regions in the interferogram: (**a**) single shot fringe pattern and (**b**) $n_{i,j}$ and parts of $p_{i,j}$.

Instead of pure tilt and tip terms, we use another aberration dominated by tilt-tip and coma as an example as shown in Figure **5**. Figure **5**(**a**) shows the single shot fringe pattern corresponding to the

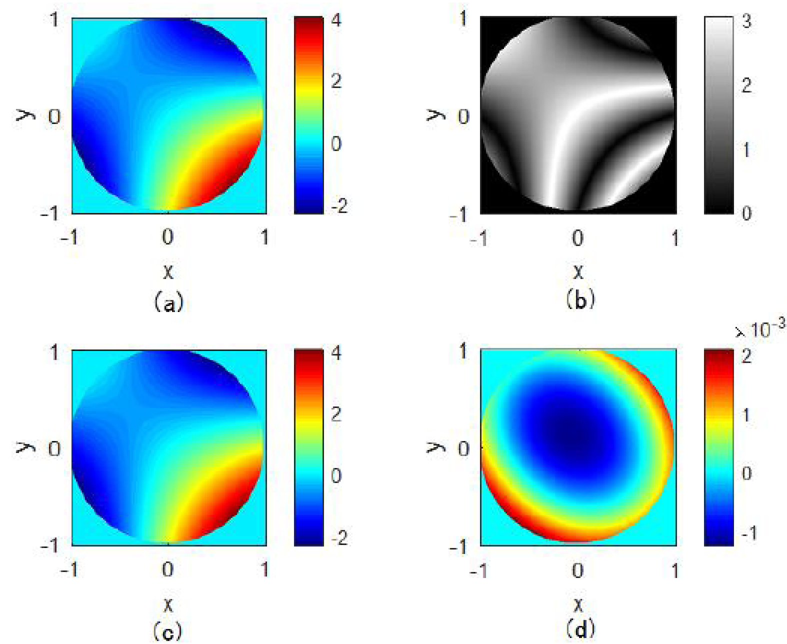

Figure 6: Single shot interferogram and its extracted phase: (**a**) original wavefront, (**b**)$\Delta\phi_\pi$, (**c**) extracted wavefront and (**d**) wavefront error, unit: rad.

aberration, and Figure **5**(**b**) shows the calculated value of $n_{i,j}$ and parts of typical $p_{i,j}$. For every pixel on the fringe pattern as shown in Figure **5**(**a**), its $p_{i,j}$ is calculated according to equation (6) from left to right and from bottom to top as described in section 2. It is obvious that the parity of $p_{i,j}$ is the same in the same region, that is ,they are odd or even in the same area. We have carried out a number of fringe pattern simulations. This parity property is suitable for their fringe patterns, such as closed and /or open fringe patterns.

Correspondingly, Figure **6** shows the simulation results, and wavefront is in unit of rad. Figure **6**(**a**) shows the original wavefront. $\Delta\Phi_\pi$ calculated from Figure **5**(**a**) is shown in Figure **6**(**b**). PV and rms of the original wavefront are 1.01l and 0.211l, respectively. After the data processing, the extracted wavefront is obtained as shown in Figure **6**(**c**). And its PV and rms are 1.01l and 0.211l, respectively. According to equation (14), the calculated wavefront error is shown in Figure **6**(**d**). And PV and rms of the residual wavefront are 0.00054l and 0.000125l, respectively. Therefore, the precision of the wavefront recovery is theoretically very high compared to the original wavefront, and the simulated error rms is less than one thousandth of a wavelength.

As a comparison, the results obtained with FFT(fast fourier transformation, FFT) method [28] are also shown in the Figure **7**. An optimized spatial frequency were added and correspondent Fourier spectra were

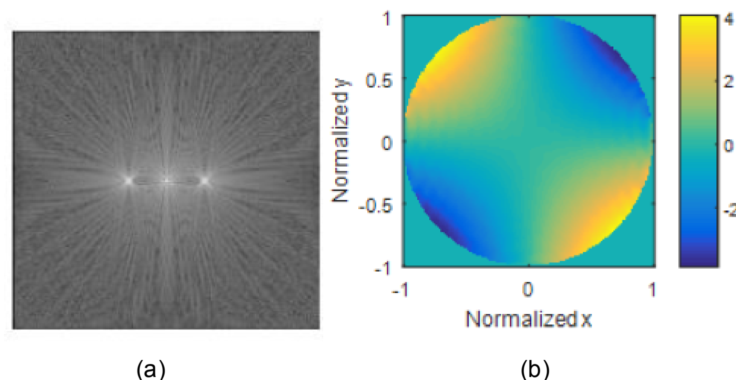

Figure 7: Results of FFT method: (**a**) Fourier spectra and (**b**) extracted wavefront, unit: rad.

shown in Figure **7**(**a**). And only left side peak is used for phase extraction. It should be noted that the tilt and tip components in the original wavefront can't be extracted with FFT method. Therefore, only high order aberrations without tilt and tip were computed as shown in Figure **7**(**b**). In addition, removing the opposite phase is necessary because of the direction uncertainty to calculate the accurate error. Compared the extracted wavefront with the original one with our tilt and tip terms, we could obtain the error wavefront. And its error PV and rms are 0.5516l and 0.0169l, respectively. Obviously, our method has a much higher precision.

In fact, there are two main factors that will deteriorate the precision of phase extraction. First, it is the noise in fringe patterns. It should be noted that the fringe patterns used in theoretical simulation do not include noise. Therefore, it will be very easy to find the peak and vale traces in the fringe pattern. Noise will lead to some fake peak or vale points, which will make the peak and vale trace very complex. Therefore, filtering is necessary for a experimental fringe pattern. Second, it is easy to introduce error at the pixels on the peak or vale trace as shown in Figure **5**(**b**). Therefore, Zernike polynomials fitting is valuable to decrease the error.

4. EXPERIMENTAL INTERFERENCE FRINGES AND PHASE RECOVERY

The interferogram acquired in lab is shown in Figure **8**(**a**). In the experimental interference fringe, data processing is important because of the noise in the fringe data as shown in Figure **8**(**a**). Therefore, it is necessary to do an image processing including filtering and normalization process of the fringe pattern so that the processed fringe pattern has a high signal to noise ratio(SNR). A high SNR image is key to improve the accuracy of phase extracting. To find the peak and vale traces accurately in the interference fringe pattern, which is very crucial to calculate $n_{i,j}$ for each pixel. From the interference fringe in Figure **8**(**a**), the wavefront to be measured is calculated as shown in Figure **8**(**b**). The unit in the wave is radians, and correspondingly PV(peak to vally, PV) and rms(root of mean square, rms) are 4.47l and 1.15l, respectively.

5. CONCLUSION

In the paper, we presented a simple and effective method theoretically and experimentally to recover the wavefront of an optical element to be tested based on a single shot fringe pattern. The theoretical simulation results show that the error is very small with PV of 0.00054λ, and rms of 0.000125λ, which are much better than those obtained with FFT method. Therefore, the accuracy of the wavefront recovery is very high. We also use the method in the experimentally measured interference fringe and estimate the shape of the optical component to be tested. During large aperture aspheric surface processing and testing, we could use the optical layout as shown in Figure **4** to get the prior knowledge. Then, it will be helpful for us to solve the global sign ambiguity and determine the reasonable and accurate wavefront of the optical element. In this case, the inclination direction of the final surface to be tested or the concave and convex direction of the curved surface can be judged reasonably. The proposed method has the following advantages: First, the hardware requirements are low: no expensive, and high precision phase shifter in the traditional phase shifting interferometer is necessary; Secondly, the calculation is simple. Complex calculations such as

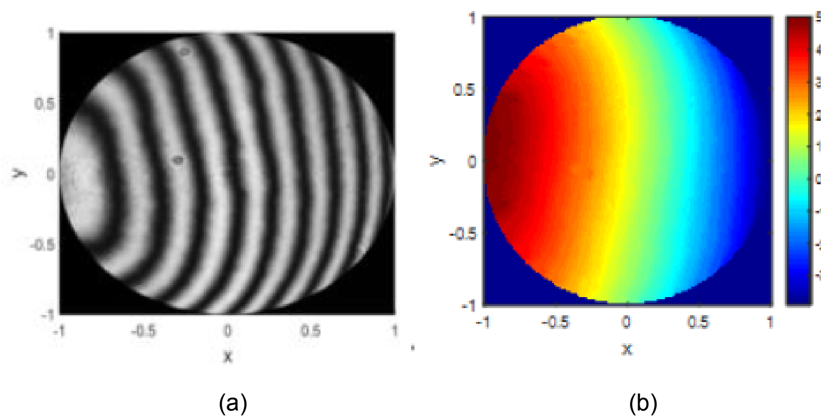

Figure 8: Interferogram obtained by experimental measurement and recovered wavefront: (**a**) interference fringe, (**b**) wavefront, unit: rad.

Fourier transform and Hilbert transform are not used; Finally, it is effective for a wide range of conditions in many applications. On the contrary, the Fourier transform method requires carrier frequency. The Hilbert transform method requires special processing for a close the interference fringe pattern. Our method does not have these limitations and is effective for complex interferogram with closed and/or open fringe patterns in applications.

DISCLOSURES

This work has no conflicts of interest.

ACKNOWLEDGMENTS

This work was supported by National Natural Science Foundation of China (61475152) and Jiangsu Six talent peaks program (GDZB-011).

REFERENCES

[1] G. M. Lai, Toyohiko and Yatagai, J. Opt. Soc. Am A, 8(5), 822-827 (1991). https://doi.org/10.1364/JOSAA.8.000822

[2] M. Born and E. Wolf, Cambridge University Press, ISBN.9781139644181, 366-420 (1999).

[3] C. Tian and S. C. Liu, Opt. Express, 24, 18695-18708 (2016). https://doi.org/10.1364/OE.24.018695

[4] H. C. Gao, Y. Jiang, L.C. Zhang and L. Jiang, Appl, Opt 57(5), 1168-1173 (2018). https://doi.org/10.1364/AO.57.001168

[5] K. M., Qian, X. P. Wu and A. Asundi, Appl. Opt, 41(13), 2448-2453 (2002). https://doi.org/10.1364/AO.41.002448

[6] Safrani and I. Abdulhalim, Opt. Lett, 39(17), 5220-5223 (2014). https://doi.org/10.1364/OL.39.005220

[7] J. Zong and J. Weng, Appl. Opt, 43, 4993-4998 (2004). https://doi.org/10.1364/AO.43.004993

[8] B. C. Chen and C. Basaran, Appl.Opt, 50(4), 586-593 (2011). https://doi.org/10.1364/AO.50.000586

[9] Ghlaifan, Y. Tounsi, D. Muhire and A. Nassim, International Journal of Optics and Applications, 7(4), 69-74 (2017).

[10] L. R. Watkins, S. M. Tan, and T. H. Barnes, Opt. Lett, 24(13), 905-907 (1999). https://doi.org/10.1364/OL.24.000905

[11] J. G. Zhong and J. W. Weng, Opt. Lett, 30(19), 2560-2562 (2005). https://doi.org/10.1364/OL.30.002560

[12] K. Pokorski and K. Patorski, Appl. Opt, 49(19), 3640-3651 (2010). https://doi.org/10.1364/AO.49.003640

[13] K. Assid, F. Alaoui, V. Dembele, S. Houmairi, M. Sidki and A. Nassim, The Open Optics Journal, 6, 9-13 (2012). https://doi.org/10.2174/1874328501206010009

[14] M. Trusiak, L. Służewski and K. Patorski, Opt. Express, 24(4), 4221-4238 (2016). https://doi.org/10.1364/OE.24.004221

[15] G. E. Galizzi, A. Federico and G. H. Kaufmann, Appl. Opt, 56(15), 4412-4418 (2017). https://doi.org/10.1364/AO.56.004412

[16] M. Takeda, H. Ina and S. Kobayashi, Journal of the optical society of America, 72(1), 156-160 (1982). https://doi.org/10.1364/JOSA.72.000156

[17] C. Roddier and F. Roddier, Appl. Opt, 26(9), 1668-1673 (1987). https://doi.org/10.1364/AO.26.001668

[18] K. M. Qian, Appl. Opt, 43(13), 2695-2702 (2004). https://doi.org/10.1364/AO.43.002695

[19] W. J. Gao, N. Thi,T. Huyen, H. S. Loi and K. M. Qian, Opt. Express, 17(25), 23147-23152 (2009). https://doi.org/10.1364/OE.17.023147

[20] M. Servin, J. L. Marroquin, D. Malacara and F. J. Cuevas, Appl. Opt, 37(10), 1917-1923 (1998). https://doi.org/10.1364/AO.37.001917

[21] M. Servin, J. L. Marroquin, and J. A. Quiroga, J. Opt. Soc. Am. A, 21(3), 411-419 (2004). https://doi.org/10.1364/JOSAA.21.000411

[22] L. Liu, Y. Y. Yang, C. Tian, Y. J. Luo and Y. M. Zhuo, Chinese J. Lasers, 37(2), 531-536 (2010). https://doi.org/10.3788/CJL20103702.0531

[23] J. M. Bioucas-Dias and G. Valadao, "Phase unwrapping via graph cuts," IEEE Trans. Image Process, 16(3), 698-709 (2007). https://doi.org/10.1109/TIP.2006.888351

[24] D. J. Wu, L. Kim, "Boyer,Sign Ambiguity Resolution for Phase Demodulation in Interferometry with Application to Prelens Tear Film Analysis," IEEE Computer Society Conference on Computer Vision and Pattern Recognition, 2807-2814 (2010).

[25] W. W. Zeng, X. P. Zhong, J. Z. Li, "Eliminating sign ambiguity for phase extraction from a single interferogram," Optical Engineering, 52(12), 124102-124112 (2013). https://doi.org/10.1117/1.OE.52.12.124102

[26] J. A. Quirogaa and M. Servin, OPT Commun, 224, 221-227 (2003). https://doi.org/10.1016/j.optcom.2003.07.014

[27] L. F. Hu, L. Xuan, Z. L. Cao, Q. Q. Mu, D. Y. Li and Y. G. Liu, Opt. Express, 14(25), 11911-11918 (2006). https://doi.org/10.1364/OE.14.011911

[28] Q. Liu, Y. Wang, J. G. He, F. Ji and B. R. Wang, "Tilt shift determinations with spatial-carrier phase-shift method in temporal phase-shift interferometry," J. Opt, 16, 075404 (2014). https://doi.org/10.1088/2040-8978/16/7/075404

Received on 24-08-2023 Accepted on 22-09-2023 Published on 26-10-2023

DOI: https://doi.org/10.31875/2409-9848.2023.10.12

© 2023 Hu *et al.*; Zeal Press.
This is an open access article licensed under the terms of the Creative Commons Attribution Non-Commercial License (http://creativecommons.org/licenses/by-nc/4.0/), which permits unrestricted, non-commercial use, distribution and reproduction in any medium, provided the work is properly cited.